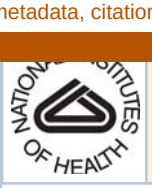

Published in final edited form as:

Colloid Polym Sci. 2012 February 1; 290(3): 221–231. doi:10.1007/s00396-011-2540-7.

A new, simple, green, and one-pot four-component synthesis of bare and poly(α,γ, L-glutamic acid)-capped silver nanoparticles

Magdalena Stevanović,
Institute of Technical Sciences of the Serbian Academy of Sciences and Arts, Knez Mihailova 35/IV, Belgrade 11000, Serbia

Igor Savanović,
Institute of Technical Sciences of the Serbian Academy of Sciences and Arts, Knez Mihailova 35/IV, Belgrade 11000, Serbia

Vuk Uskoković,
Therapeutic Micro and Nanotechnology Laboratory, Department of Bioengineering and Therapeutic Sciences, University of California, San Francisco, CA 94158, USA

Srečo D. Škapin,
Advanced Materials Department, Jožef Štefan Institute, Jamova 39, Ljubljana 1000, Slovenia

Ines Bračko,
Advanced Materials Department, Jožef Štefan Institute, Jamova 39, Ljubljana 1000, Slovenia

Uroš Jovanović, and
Chemical Dynamics Laboratory, The Vinca Institute of Nuclear Sciences, P.O. Box 522, 11001, Belgrade, Serbia

Dragan Uskoković
Institute of Technical Sciences of the Serbian Academy of Sciences and Arts, Knez Mihailova 35/IV, Belgrade 11000, Serbia

Magdalena Stevanović: magdalena.stevanovic@itn.sanu.ac.rs

Abstract

A simple and green chemical method has been developed to synthesize stable bare and capped silver nanoparticles based on the reduction of silver ions by glucose and capping by poly(α, γL-glutamic acid) (PGA). The use of ammonia during synthesis was avoided. PGA has had a dual role in the synthesis and was used as a capping agent to make the silver nanoparticle more biocompatible and to protect the nanoparticles from agglomerating in the liquid medium. The synthesized PGA-capped silver nanoparticles in the size range 5–45 nm were stable over long periods of time, without signs of precipitation. Morphological examination has shown that the silver nanoparticles had a nearly spherical, multiply twinned structure. The effects of the reaction temperature and the reaction time during the synthesis were investigated too. The biocompatibility of the PGA-capped silver nano-particles is discussed in terms of in vitro toxicity with human intestinal Caco-2 cells. The samples were characterized by UV–Visible spectroscopy, field emission scanning electron microscopy, transmission electron microscopy, and zeta potential measurements.

Correspondence to: Magdalena Stevanović, magdalena.stevanovic@itn.sanu.ac.rs.

Keywords

Silver nanoparticles; Green method; Poly(α, γL-glutamic acid); Capping agent; In vitro toxicity

Introduction

Scientific and commercial interest in the manufacture of nanostructured materials has significantly increased since the discovery of their importance for numerous uses. Noble metal nanoparticles find many applications in different technological areas due to their unique optical, electronic, mechanical, magnetic, and chemical properties that are drastically different from those of the corresponding bulk materials [1–3]. There have been numerous recent reports on the fabrication of silver nanoparticles. It has attracted particularly considerable attention due to the diverse properties and applications of silver nanoparticles, including magnetic and optical polarizability, electrical conductivity, catalysis, antimicrobial behavior, DNA sequencing, surface-enhanced Raman scattering, and thermal properties [4]. The literature describes different methods for obtaining silver nanoparticles, such as chemical reduction method, solid-state synthesis, sonochemical synthesis, in situ radical polymerization, spray pyrolysis, etc. [5–11]. By optimizing experimental conditions, such as the concentrations of reactants, temperature, pH, reducing agents, different surfactants, and the reaction medium, it is possible to synthesize nanoparticles of different sizes and morphology and significantly affect the stability of the resulting particles [12, 13].

Nanosilver is reported to be used in many applications, but in the literature, it has also been reported that bare silver nanoparticles can be toxic [14]. This supports the idea that the toxicity is associated with the presence of bare metallic nanoparticle surfaces [15, 16], while particles protected by the organic layer (tiopronin [17], bovine serum albumin [18], Na^+–poly(γglutamic acid) [19], etc.) are much more biocompatible and thereby less toxic, except starch-capped nanoparticles which present mitochondrial dysfunction, induction of reactive oxygen species, DNA damage, and cell cycle arrest [20]. The toxicology and toxicokinetics of nanosilver was extensively reviewed by Johnston et al. [21], and the main points of relevance for risk assessment were summarized in the paper of Christensen et al. [22]. Since noble metal nanoparticles are widely applied in areas of human contact [23], there is a growing need to develop environment-friendly processes for nanoparticle production that do not rely on toxic chemicals. The synthesis of nanomaterials in an environmental benign way is certainly a challenge [24]. The principles of green chemistry include the adoption of less hazardous syntheses; selection of safer starting materials with a good degree of utilization; avoidance of the use of toxic solvents; usage of renewable, biodegradable materials; and minimized energy requirements. The great industrial and technological impact on human life and nature are in demand of continuous improvements and innovations, which are followed by the increase of green chemistry patents, all over the world [24, 25].

In this study, we have focused on developing a green chemical synthesis of stable suspensions of silver nano-particles. A variety of chemical reduction syntheses have already been developed to produce silver nanoparticles, though mainly involving ammonia [26]. Although in wide use, ammonia is both caustic and hazardous. It is a corrosive chemical that will per se destroy or irreversibly damage another surface or substance with which it comes into contact. The main hazards to people include damage to the eyes, the skin, and the tissue under the skin; inhalation or ingestion of a corrosive substance can damage the respiratory and gastrointestinal tracts [27].

Herein, we demonstrate a simple and quick synthesis of uniform, stable silver nanoparticles using glucose as the reduction agent, poly(α, γL-glutamic acid) (PGA) as the capping agent,

and without using ammonia in the synthesis. The choice of an appropriate stabilizer and reducing agent for the preparation of stable colloidal silver nanoparticles is very important.

A number of researchers have reported on the successful synthesis of Ag nanoparticles, but the use of this green, one-pot, four-component method overcomes in great extent some of the disadvantages previously reported by other methods, such as impurities, solvent toxicity, size and distribution control, long tedious process, economic viability, and difficulty in their preparation that limits their commercialization potential [5–13, 28, 29]. The major advantage of this processing of the silver nanoparticles, relative to other methods, is most certainly due to the use of PGA as the capping agent.

The use of PGA as a capping agent is already reported by another group [19], but with the use of ammonia in the synthesis, which was avoided in our method. On the other hand, the use of ammonia, which is a hazardous chemical, was avoided in a number of other methods, but with use of other chemicals as reducing and/or capping agents (sodium borohydride, dimethyl formamide, cetyltrimethylammonium bromide, starch, etc.) [5, 20, 28, 30], for which there is a general concern that they pose potential environmental and biological risks.

Poly(α, γL-glutamic acid) is a hydrophilic, biodegradable, and naturally available biopolymer usually produced by various strains of *Bacillus* [31]. Its biological properties such as non-toxicity, biocompatibility, and non-immunogenicity qualify it as an important biomaterial for applications in medicine, pharmaceutics, cosmetics, food industry, and others. In addition, poly(α, γL-glutamic acid) is a biodegradable macromolecule developed rapidly in the last two decades. The incorporation of PGA into the antigenic formulation, influenza vaccine, and gene transfection carrier improved the pharmaceutical efficacies [31]. If, for example, silver nanoparticles are intended for use in biomedical purposes, PGA can ensure a more favorable interaction of the nanoparticles with living cells and at the same time can act as a particle stabilizer [31].

It is now known that besides nanoparticle size and composition, particle shape could play a critical role in their application, notably in interaction with cells, in modulating their optical and catalytic properties, etc. [32]. Multiply twinned particles are the naturally abundant seed morphology, but because of their twin defects, they are also the most reactive particles [32, 33]. This type of nanoparticle substructure thus has the potential of furthermore increasing nanoparticle reactivity due to their high surface area. The method described herein provides a generally high-yield, low-cost route to the preparation of multiply twinned, stable silver nanoparticles capped with a biocompatible polymer. Only four components were used for the preparation of the particles: sodium hydroxide, glucose, silver nitrate, and poly(α, γL-glutamic acid). No other ion is introduced to the reaction, making the subsequent separation particularly facile. The whole preparation is complete in a single reaction vessel which facilitates fabrication. The effects of the reaction temperature and reaction time were investigated, and the possible formation mechanism of silver nano-particles in this synthesis was discussed. Synthesized nanoparticles were characterized by UV–Visible spectroscopy, field emission scanning electron microscopy (FESEM), transmission electron microscopy (TEM), and zeta potential measurements. As a part of this study, we also examined the effect the silver nanoparticles had on the integrity of the human intestinal epithelial layers in culture. Caco-2 cells have been previously proven as a useful model for the in vitro investigation of drug delivery systems [34–37]. Hereby, we merely aimed at looking at possible toxic effects on the cell density and the disruption of the tight junction which is vital for the healthy paracellular transport of molecules across the epithelium.

Experimental procedures

Materials

Silver nitrate ($AgNO_3$, M_r=169.88) was obtained from Centrohem (Serbia), glucose ($C_6H_{12}O_6$, M_r=180.20) from Zorka Pharma (Serbia), and sodium hydroxide (NaOH, M_r= 40.00) was acquired from Kemika (Croatia). PGA with M_w= 20–40 kDa (99.9% HPLC purity) were purchased from Guilin Peptide Technology Limited (China). All reagents were of analytical grade and were used as received without further purification.

Methods

Green synthesis of bare and poly(α,γ, L-glutamic acid)-capped silver nanoparticles—Bare and capped silver nanoparticles were synthesized in the new, simple, green chemical manner, i.e., by a chemical reduction method wherein silver nitrate, glucose, and poly (α, γL-glutamic acid) served as a precursor, a reduction agent, and a capping agent, respectively (Fig. 1). The initial solution in all syntheses was 20 mL distilled water, in which 0.5 mL of (0.5 wt.%) NaOH and 10 mL of (1 wt.%) glucose were introduced, with continuous stirring on a magnetic stirrer at 300 rpm. The reaction temperature and the reaction time were varied in order to examine their influence on the formation of silver nanoparticles. For the formation of capped silver nanoparticles, 0.5 mL of (0.1 wt.%) PGA was added into the solution before adding 0.5 mL of $AgNO_3$ (0.1 wt.%). Glucose in an alkaline solution is slowly oxidized by oxygen, forming gluconic acid. In the presence of sodium hydroxide, gluconic acid is converted to sodium gluconate. Silver nitrate speeds up the reaction by acting as an oxidizing agent. As glucose is oxidized by the dissolved oxygen, silver ions are reduced, forming silver nanoparticles, and the yellow green color of the solution appears. The formation of silver nanoparticles can be observed by a change in color since small nanoparticles of silver are yellow green due to a phenomenon known as surface plasmon resonance (SPR). The addition of PGA prevents the agglomeration of the nanoparticles. A layer of absorbed glutamic acid anions on the surface of the silver nanoparticles keeps the nanoparticles separated. The solution was stirred for over 3 h to ensure that the reaction had been completed.

UV spectroscopy—UV measurements were performed on a GBC Cintra UV–Vis spectrophotometer in the wavelength range of 200–600 nm. UV spectroscopy has been used to estimate the formation of silver nanoparticles during the reaction, the formation of PGA-capped silver nanoparticles, the stability of silver nanoparticles over time, and also the influence of different processing parameters during the synthesis.

Field emission scanning electron microscopy—To clarify the microstructure of bare and capped silver nanoparticles, FESEM observation was carried out. FESEM measurements were performed on a SUPRA 35 VP Carl Zeiss field emission scanning electron microscope. The samples were prepared by re-dispersing them in ethanol by means of ultrasonic irradiation and filtering the dispersions using polycarbonate membranes. Carbon coating was used to prevent charging.

Transmission electron microscopy—TEM using JEOL JEM-2100 was employed for further morphological characterization of PGA-capped silver nano-particles. The structural characteristics of silver nanoparticles were determined by selected-area electron diffraction (SAED) and high-resolution transmission microscopy (HRTEM). Samples for the TEM analysis were prepared by dispersing the powders in distilled water using an ultrasonic bath. Suspensions were subsequently dropped on a lacey carbon film supported by a 300-mesh copper grid.

Zeta potential measurements—Zeta potential was measured on a Zetasizer (Nano ZS, model ZEN3600; particle size range for zeta potential determination, 5 nm–10 μm; Malvern Instruments, Malvern, UK) using the principles of electrophoretic mobility in an electric field. Zeta potential is the function of pH which determines particle stability in dispersion.

Caco-2 cell culture—Human intestinal Caco-2 cells were grown and maintained at 37°C in an atmosphere of 5% CO_2/95% air at 90% relative humidity. In all experiments, Caco-2 cells were seeded in 24-well plates at the density of 7.5×10^4 cells per well on microscope cover glass slides (Fisherbrand). The cell culture media composed of (a) Eagle's minimum essential medium (450 mL, UCSF Cell Culture Facility) with Earle's balanced salt solution, 2 mM L-glutamine, 0.1 mM nonessential amino acids, and 1.5 g/L sodium bicarbonate; (b) 1 mM sodium pyruvate; (c) 20% fetal bovine serum; and (d) 1% penicillin–streptomycin antibiotic solution, which was replaced every 2 days.

Immunofluorescence for zonula occludens-1 and f-actin—After reaching confluency, the cells were exposed apically to 300 μL of the stable suspension of PGA-capped silver nanoparticles and 500 μL of the cell culture media added to the cell culture wells and then aged for 5 h at 37 °C. The media with suspended particles were then aspirated and the cells washed with phosphate buffer solution (PBS, pH 7.4) and fixed for 15 min in 3.7% paraformaldehyde. The cells were then washed three times with PBS, 5 min each, and then with the blocking solution (PBT=1% bovine serum albumin, 0.1% Triton X-100 in PBS) two times, 5 min each. The cells were then blocked and permeabilized in PBT for 1 h and then incubated in 200 μL per well of the primary anti-zonula-occludens-1 (ZO-1) antibody immunoglobulin G (IgG) (rabbit anti-ZO1 Zymed Lab) in PBT overnight and washed with PBS three times for 10 min. The cells were then incubated in 150 μL aqueous solution of the secondary antibody (AlexaFluor 555 goat anti-rabbit IgG, Invitrogen), phalloidin-tetramethylrhodamine (AlexaFluor 488, Invitrogen), and 4′,6-diamidino-2-phenylindole dihydrochloride nuclear counterstain (DAPI 405, Invitrogen), all in PBT, and then washed with PBS three times for 5 min. The coverslips containing the fixed and stained cells were mounted onto glass slides using vectashield and nail polish and imaged in oil on the spectral confocal laser scanning microscope, C1si (UCSF Nikon Imaging Center), at ×60 magnification. All the experiments were done in triplicate, and staining immunofluorescence was analyzed at approximately ten randomly selected images in each sample. Volume-rendered *z*-stack images (12–15 of them) spaced by 1 μm were collected at identical laser intensities and analyzed for cell count and average pixel intensity using ImageJ Software.

Results and discussion

UV spectroscopy

UV–Visible spectroscopy is one of the most widely used techniques for the structural characterization of silver nanoparticles [38]. This is so because silver nanoparticles exhibit an intense absorption band due to SPR [38].

The UV spectroscopy results shown in Fig. 2 indicated the formation of bare silver nanoparticles as well as of silver nanoparticles capped with PGA. After adding $AgNO_3$ to the reaction mixture, the color of the solution turned yellow, which indicated the formation of silver nanoparticles. Figure 2a–c shows volumetric flasks containing the negative control (all components without $AgNO_3$), solution with $AgNO_3$ but without PGA, and all components including $AgNO_3$ and PGA after completion of the reaction, respectively. The flasks containing $AgNO_3$ and Ag + PGA solutions exhibit a gradual change in the color of the reaction mixture from colorless to yellow green without the color intensity increasing after 90 min of reaction time. The negative control does not show the characteristic change

in color. From the changes in the solution color and spectra measurements, we may conclude that the reaction is completed within a total of 90 min under magnetic stirring. This is evidenced by the absence of color change after 90 min of stirring and by observing the final product having a yellow green color that persisted even after an extended period of stirring.

The UV/Vis absorption spectra (Fig. 2) of silver particles, synthesized using PGA as a stabilizer, display a narrow surface plasmon absorption band at λ=408 nm. In the case of bare silver nanoparticles, obtained from the reaction with the same duration time (90 min) but without adding PGA, the absorption band is at 421 nm, which means that the particles obtained with PGA as a stabilizer have smaller sizes [39]. The blue shift of the plasmon resonance from 421 to 408 nm is due to the change in the local refractive index of nanoparticles resulting from the interaction between PGA and the metal surface [40, 41].

Besides the shift, broadening of the plasmon peak in the case of silver particles obtained without PGA was also observed (Fig. 2a). The broadened peak indicates that the particles obtained without PGA are also in the nanoregime. However, peak broadening may also signify the possibility of the presence of particles with different sizes. Such broadening might be caused by the agglomeration of silver particles; the main reason for this phenomenon is the lack of a stabilizer in the experiment.

Temperature effect during the green and one-pot, four-component synthesis of silver nanoparticles—As shown in Fig. 3, the intensity of the surface plasmon absorption band increases as the reaction temperature increases, thus indicating the continued reduction of silver ions, i.e., a continued increase in the concentration of silver nanoparticles [42]. When the reaction temperature reaches 90 °C (Fig. 3), the intensity of the plasmon absorption band is increased and the λ_{max} value is slightly red-shifted from 404 to 408 nm. This indicates an increase in the particle size. The absorbance peak, due to the surface plasmon resonance effect of metallic nanoparticles, is known to undergo a red shift following the particle size increase [39].

For the reaction temperature of 100 °C, the absorbance also increased, but without any further shift in the peak position. Reduction of Ag^+ ions leads to the formation of nuclei. The structure of the nuclei fluctuates in relation to their size and the thermal energy available. In this case, this phenomenon is more pronounced at temperatures around 90 °C. As the nuclei grow, fluctuations stop and the structure becomes confined in a multiply twinned, singly twinned, or single-crystal seed [33].

Time-dependent effect in green and one-pot, four-component synthesis of silver nanoparticles—The synthesized PGA-capped silver nanoparticles (T=100 °C) were simultaneously characterized by UV–Vis spectroscopy measurements performed at different time intervals to study the change in the light absorption profile of the solution and the increase in intensity. The absorption spectra of nano-particles show highly symmetric single-band absorption with the peak maximum at 408 nm. Peak intensity steadily increases as a function of the reaction time without any shift in the peak wavelength (Fig. 4). This indicates the presence of silver nanoparticles at the earliest reaction time points, demonstrating that even 1 min of the reaction time is enough for the particles to form. After 90 min of reaction time, no further increase in intensity is detected (120 and 180 min), indicating complete reduction of precursor silver ions.

Although it would be expected that the reduction reaction will be faster in the initial stage and gradually slows down, this trend is not observed, and this is in agreement with the findings of other authors [29, 43, 44].

In aqueous solution, the stabilizer (capping agent) plays an important role in determining not only the stability and size of the silver nanoparticles but also the mechanism and kinetics of their formation [43, 44]. The absorbance intensity vs. the reaction time in the different stabilizers and the silver salt weight ratio are already described in the literature [44]. It comes out that the starting concentrations of the stabilizer determine the maximum extent that the reduction can reach in each case, i.e., the reduction rate is strongly influenced by the weight fraction of the stabilizer in the stabilizer/precursor ratio.

Stability of the samples 3 months after synthesis—After the as-synthesized PGA-capped silver nanoparticles (obtained at T=60 °C and 100 °C) underwent a 3-month storage period in suspension, their UV–Vis spectra were measured and are displayed in Fig. 5. The spectra had very similar UV–Vis absorption curves as those obtained immediately after preparation. The unchanged peak shape and position indicates no change in the size of the particles, nor an occurrence of their agglomeration. The absorption spectra of the solutions containing AgNpPGA particles recorded immediately after the preparation and after 3 months confirmed the very good stability of the samples (Fig. 5).

Field emission scanning electron microscopy

The morphological characteristics of the bare and capped silver nanoparticles, obtained in the experiment with reaction time 90 min and reaction temperature 100 °C, have been examined using field emission scanning electron microscope. By using PGA as the stabilizer, the samples with different morphological characteristics, at macroscopic and microscopic scales alike, were obtained. From Fig. 6, it can be noticed that bare silver particles have spherical but also irregular shapes and are not very uniform. From the micrograph of the bare silver nanoparticles, it is also visible that the particles are quite agglomerated. The main reason for this phenomenon is the missing stabilizer in the experiment.

FESEMs of the bare and capped silver nanoparticles show a considerable difference. From the FESEM imaging of capped particles (Fig. 7), it is visible that the particles possess spherical shapes, smooth surfaces, low levels of agglomeration, and high levels of uniformity—higher than bare silver nanoparticles. By introducing PGA into the solution mixture, silver nanoparticles become more uniform, thanks to the surface layer of the biopolymer (arbitrarily magnified particle—whitish circle, Fig. 7). This PGA lining provides better biocompatibility of AgNps and also makes the particles separated. The size distribution of all nanoparticles is unimodal, with sizes in the range of 5–45 nm.

Transmission electron microscopy

The silver nanoparticles obtained without and with PGA were also examined by TEM. TEM studies of the silver nanoparticles obtained in the experiment without PGA revealed the irregular morphology of the particles. From Fig. 8a, it can be seen that lack of the stabilizer in the system leads to the formation of agglomerates and particles with a broad size distribution.

Further analyses of the PGA-capped silver nanoparticles using TEM show mostly twinned nanoparticles present in the sample. As already mentioned, multiply twinned particles are the naturally abundant seed morphology, but because of their twin defects, they are also the most reactive [33]. Much effort has gone into generating polyhedral noble metal nanostructures because of their superior performance in a variety of applications ranging from catalysis to electronics, surface plasmon resonance, surface-enhanced Raman scattering, and biomedical research [29, 45]

Figure 8 shows typical low-magnification TEM images of the silver nanoparticles prepared at 100 °C. Most of the nanoparticles are well-refined decahedrons and icosahedrons with sizes ranging from 5 to 45 nm. The size of the particles is defined here as the distance from one edge of the projection to the opposite edge. Typical SAED patterns of AgNp and AgNpPGA nanoparticles in Fig. 8 reveal the coexistence of Ag nanoparticles with cubic and hexagonal crystal structures [46, 47]. Figure 9 shows a high-resolution TEM image of a typically multiply twined silver nano-particle. A multiply twinned boundary at the center of a silver nanoparticle can be clearly observed from various angles; the lattice plane is separated by a twin boundary indicated as a line on the image. The formation of multiply twinned silver nanoparticles has already been described in the literature [29, 33]. In the early stage of the reaction, silver ions are reduced to neutral atoms, which in turn come together to form nuclei. When the nuclei are sufficiently small, the available thermal energy causes their structure to fluctuate, allowing defects to form or be removed depending upon their energetic favorability [48]. Most silver nuclei incorporate twin boundary defects because such defects enable a lower surface energy [49]. As the nuclei grow, changes in the defect structure become too costly relative to the available thermal energy, and they become confined within a given morphology. This process results in a Boltzmann-like distribution of multiply twinned, singly twinned, and single-crystal seeds, with the fivefold twinned decahedron being the lowest in free energy and thus the most abundant morphology [50]. This variety of seeds grows to form nanostructures with different shapes. Therefore, the growth of a silver nanocrystal during the synthesis can be divided into three stages: nucleation (reduction of metal ions to zerovalent atoms), seeding (evolution from nuclei to seeds), and growth (evolution from seeds to nanocrystals) [51].

Zeta potential measurement

The results of the determination of the zeta potential of bare and PGA-capped silver nanoparticles are shown in Table 1. The zeta potential was reported as the average of $n=5$ (five readings taken per sample), including the standard deviation. PGA was used as a stabilizer, which creates negatively charged silver particles, endowing the particles with a specific zeta potential. The zeta potential is an important property of dispersed particles as it is a measure of their electrostatic repulsion and, hence, their stability. Theoretically, the zeta potential stabilizes suspensions whether the value is positive or negative, so long as the absolute value exceeds 15–30 mV depending on the type of dispersion [52]. The measured values of the particles size are lower for silver nanoparticles stabilized and capped with PGA compared with the bare ones, which is in a good agreement with FESEM images. Although the PGA layer adds up to the size of the particles, this serves as an evidence of the reduction in the particle size that it promotes as an additive during the precipitation of silver nanoparticles, presumably by adsorbing onto the growing particle facets. Values of the zeta potential of all samples are higher than −30 mV, indicating good stability of the colloidal system [52]. The polydispersity index (PDI), which is a dimensionless number indicating the width of the size distribution, with a value between 0 and 1 (0 for monodisperse particles), is also obtained and presented (Table 1).

Determining cytotoxicity of the synthesized PGA-capped silver nanoparticles

Figure 10 displays volume-rendered confocal images of Caco-2 epithelial cell layers imaged after incubation with the silver nanoparticles coated with PGA. Comparison with the untreated, negative control images suggests no detectable damaging effects either to the tight junction or to the cell viability. Figure 11 shows a statistically insignificant change in the live cell count per surface area following incubation with the nanoparticles. Hence, neither a marked change in the density of the cell layer nor in the integrity of the cobblestone ZO-1 pattern was observed, suggesting no negative effects exerted on the cells by the given particles under the in vitro testing conditions applied herein. As demonstrated in Fig. 12,

although the tight junction appears ruffled after the incubation with the silver nanoparticles, the average pixel intensity of ZO-1-tagged fluorescent IgG, which is indicative of the amount of fluorescently tagged macromolecules, has remained unchanged significantly. The cytoskeletal distribution of f-actin was mildly modified in comparison with the control, from fibers traversing through the cytoplasm to their partial detraction toward the tight junction, which is consequential to the mechanochemical stress imposed by the nanoparticles onto the membrane. Actin ceases to exist in well-defined bundles, as apparent in the control sample, which may be the consequence of the uptake of the nanoparticles by the cells through endocytosis and their intracellular localization.

Conclusion

An eco-friendly, one-pot, four-component synthesis of silver nanoparticles is presented in this work. Thanks to its simplicity, the synthesis reported is very fast, cheap, and, what is most important, completely based on the principles of green chemistry. Poly(α, γL-glutamic acid), a naturally occurring anionic polymer, was used as the organic layer to protect the silver nanoparticles from agglomeration and render them biocompatible, while glucose was used as a reducing agent. The use of ammonia during the synthesis was avoided. The synthesized silver/poly(α, γL-glutamic acid) nanoparticles were highly stable in suspension over prolonged periods of time, without any signs of phase segregation. The synthesized PGA-capped nanoparticles are uniform and have a narrow particle size distribution, with the smallest average particle diameter of about 5 nm. Morphological examination has shown that the obtained silver nanoparticles had nearly spherical multiply twinned structures, which is promising for a variety of applications, ranging from catalysis to electronics, surface plasmon resonance, surface-enhanced Raman scattering, and biomedical research. It was also shown that PGA-capped silver nanoparticles are biocompatible and do not induce a toxicological response of Caco-2 epithelial cells in vitro. These results are very encouraging for future applications of silver nanoparticles.

Acknowledgments

This study was supported by the Ministry of Science and Technological Development of the Republic of Serbia, under Grant No. III45004: Molecular designing of nanoparticles with controlled morphological and physicochemical characteristics and functional materials based on them. Desai Lab at UCSF is also acknowledged for support and NIH grant K99-DE021416. Confocal microscopy data for this study were acquired at the Nikon Imaging Center at UCSF.

References

1. Sau TK, Rogach AL, Jäckel F, Klar TA, Feldmann J. Properties and applications of colloidal nonspherical noble metal nanoparticles. Adv Mater. 2010; 22(16):1805–1825. [PubMed: 20512954]
2. Ansari AA, Alhoshan M, Alsalhi MS, Aldawayyan AS. Prospects of nanotechnology in clinical immunodiagnostics. Sensors. 2010; 10:6535–6581. [PubMed: 22163566]
3. Kausch-Blecken von Schmeling HH. Eighty years of macro-molecular science: from birth to nano-, bio- and self-assembling polymers—with slight emphasis on European contributions. Colloid Polym Sci. 2011; 289(13):1407–1427.
4. Zhang WC, Wu XL, Chen HT, Gao YJ, Zhu J, Huang GS, Chu PK. Self-organized formation of silver nanowires, nanocubes and bipyramids via a solvothermal method. Acta Mater. 2008; 56:2508–2513.
5. Khan Z, Al-Thabaiti SA, Obaid AY, Al-Youbi AO. Preparation and characterization of silver nanoparticles by chemical reduction method. Colloids Surf B Biointerfaces. 2011; 82(2):513–517. [PubMed: 21050730]

6. Debnath D, Kim C, Kim SH, Geckeler KE. Solid-state synthesis of silver nanoparticles at room temperature: poly(vinylpyrrolidone) as a tool. Macromolecular Rapid Communications. 2010; 31(6):549–553. [PubMed: 21590940]
7. Zhu YP, Wang XK, Guo WL, Wang JG, Wang C. Sonochemical synthesis of silver nanorods by reduction of silver nitrate in aqueous solution. Ultrason Sonochem. 2010; 17(4):675–679. [PubMed: 20149712]
8. Xu H, Suslick KS. Sonochemical synthesis of highly fluorescent Ag nanoclusters. ACS Nano. 2010; 4:3209–3214. [PubMed: 20507161]
9. Cheng Y-J, Zeiger DN, Howarter JA, Zhang X, Lin NJ, Antonucci JM, Lin-Gibson S. In situ formation of silver nanoparticles in photocrosslinking polymers. J Biomed Mater Res B Appl Biomater. 2011; 97B(1):124–131. [PubMed: 21290590]
10. Vodnik VV, Bozanic DK, Dzunuzovic E, Vukovic J, Nedeljkovic JM. Thermal and optical properties of silver–poly(methyl-methacrylate) nanocomposites prepared by in-situ radical polymerization. Eur Polym J. 2010; 46:137–144.
11. Kieda N, Messing GL. Preparation of silver particles by spray pyrolysis of silver–diammine complex solutions. J Mater Res. 1998; 13(6):1660–1665.
12. Yin Y, Li Z-Y, Zhong Z, Gates B, Xia Y, Venkateswaran S. Synthesis and caracterization of stable aqueous dispersion of silver nanoparticles through the Tollens process. J Mater Chem. 2002; 12:522–527.
13. Le AT, Le TT, Tam PD, Huy PT, Huy TQ, Hieu N, Kudrinskiy AA, Krutyakov YA. Synthesis of oleic acid-stabilized silver nanoparticles and analysis of their antibacterial activity. Mater Sci Eng C. 2010; 30:910–916.
14. Schrand AM, Rahman MF, Hussain SM, Schlager JJ, Smith DA, Syed AF. Metal-based nanoparticles and their toxicity assessment. WIREs Nanomedicine and Nanobiotechnology. 2010; 2:544–568. [PubMed: 20681021]
15. Kim S, Choi JE, Choi J, Chung KH, Park K, Yi J, Ryu DY. Oxidative stress-dependent toxicity of silver nanoparticles in human hepatoma cells. Toxicol Vitr. 2009; 23(6):1076–1084.
16. Hussain SM, Hess KL, Gearhart JM, Geiss KT, Schlager JJ. In vitro toxicity of nanoparticles in BRL 3A rat liver cells. Toxicol Vitr. 2005; 19(7):975–983.
17. Castillo PM, Herrera JL, Fernandez-Montesinos R, Caro C, Zaderenko AP, Mejias JA, Pozo D. Tiopronin monolayer-protected silver nanoparticles modulate IL-6 secretion mediated by Toll-like receptor ligands. Nanomedicine (Lond). 2008; 3(5):627–635. [PubMed: 18834270]
18. Singh AV, Patil R, Kasture MB, Gade WN, Prasad BL. Synthesis of Ag–Pt alloy nanoparticles in aqueous bovine serum albumin foam and their cytocompatibility against human gingival fibroblasts. Colloids Surf B Biointerfaces. 2009; 69(2):239–245. [PubMed: 19131222]
19. Yu D-G. Formation of colloidal silver nanoparticles stabilized by Na^+–poly(γglutamic acid)–silver nitrate complex via chemical reduction process. Colloids Surf B Biointerfaces. 2007; 59:171–178. [PubMed: 17583483]
20. AshaRani PV, Low Kah Mun G, Hande MP, Valiyaveettil S. Cytotoxicity and genotoxicity of silver nanoparticles in human cells. ACS Nano. 2009; 3(2):279–290. [PubMed: 19236062]
21. Johnston HJ, Hutchison GR, Christensen FM, Hankin S, Peters S, Stone V. A review of the in vivo and in vitro toxicity of silver and gold particulates: particle attributes and biological mechanisms responsible for the observed toxicity. Crit Rev Toxicol. 2010; 40(4):328–346. [PubMed: 20128631]
22. Christensen FM, Johnston HJ, Stone V, Aitken RJ, Hankin S, Peters S, Aschberger K. Nano-silver feasibility and challenges for human health risk assessment based on open literature. Nanotoxicology. 2010; 4(3):284–295. [PubMed: 20795910]
23. Song JY, Kim BS. Rapid biological synthesis of silver nanoparticles using plant leaf extracts. Bioprocess Biosyst Eng. 2009; 32 (1):79–84. [PubMed: 18438688]
24. Warner JC, Cannon AS, Dye KM. Green chemistry. Environmental Impact Assessment Review. 2004; 24:775–799.
25. Nameroff TJ, Garant RJ, Albert MB. Adoption of green chemistry: an analysis based on US patents. Res Policy. 2004; 33:959–974.

26. Kuai L, Geng B, Wang S, Zhao Y, Luo Y, Jiang H. Silver and gold icosahedra: one-pot water-based synthesis and their superior performance in the electrocatalysis for oxygen reduction reactions in alkaline media. Chemistry: A European Journal. 2011; 17:3482–3489.
27. Agency for Toxic Substances and Disease Registry. Toxicological profile for ammonia. U.S. Department of Health and Human Services, Public Health Service; Atlanta, GA: 2004 Sep.
28. Singh M, Sinha I, Mandal RK. Role of pH in the green synthesis of silver nanoparticles. Mater Lett. 2009; 63:425–427.
29. Darroudi M, Ahmad MB, Zamiri R, Zak AK, Abdullah AH, Ibrahim NA. Time-dependent effect in green synthesis of silver nanoparticles. Int J Nanomedicine. 2011; 6:677–681. [PubMed: 21556342]
30. El-Shishtawy RM, Asiri AM, Al-Otaibi MM. Synthesis and spectroscopic studies of stable aqueous dispersion of silver nano-particles. Spectrochim Acta A Mol Biomol Spectrosc. 2011; 79:1505–1510. [PubMed: 21703920]
31. Shih IL, Van YT. The production of poly-(γglutamic acid) from microorganisms and its various applications. Bioresour Technol. 2001; 79:207–225. [PubMed: 11499575]
32. Marks LD, Howie A. Multiply-twinned particles in silver catalysts. Nature. 1979; 282:196–198.10.1038/282196a0
33. Wiley B, Sun Y, Xia Y. Synthesis of silver nanostructures with controlled shapes and properties. Accounts of Chemical Research. 2007; 40:1067–1076. [PubMed: 17616165]
34. Moyes SM, Morris JF, Carr KE. Macrophages increase microparticle uptake by enterocyte-like Caco-2 cell monolayers. J Anat. 2010; 217:740–754. [PubMed: 20880316]
35. Yu D, Marchiando AM, Weber CR, Raleigh DR, Wang Y, Shen L, Turner JR. MLCK-dependent exchange and actin binding region-dependent anchoring of ZO-1 regulate tight junction barrier function. PNAS. 2010; 107(18):8237–8241. [PubMed: 20404178]
36. Neumeyer A, Bukowski M, Veith M, Lehr C-M, Daum N. Propidium iodide labeling of nanoparticles as a novel tool for the quantification of cellular binding and uptake. Nanomedicine: Nanotechnology, Biology and Medicine. 2011; 4(7):410–419.10.1016/j.nano.2010.12.007
37. Bimbo LM, Mäkilä E, Laaksonen T, Lehto V, Salonen J, Hirvonen J, Santos HA. Drug permeation across intestinal epithelial cells using porous silicon nanoparticles. Biomaterials. 2011; 32 (10): 2625–2633. [PubMed: 21194747]
38. Sönnichsen C, Franzl T, Wilk T, von Plessen G, Feldmann J. Plasmon resonances in large noble-metal clusters. New J Phys. 2002; 4:93.1–93.8.
39. Heath JR. Size-dependent surface-plasmon resonances of bare silver particles. Physical Review B. 1989; 40:9982–9985.
40. Hao E, Schatz GC. Electromagnetic fields around silver nanoparticles and dimmers. J Chem Phys. 2004; 120(1):357–366. [PubMed: 15267296]
41. Potara M, Jakab E, Damert A, Popescu O, Canpean V, Astilean S. Synergistic antibacterial activity of chitosan–silver nano-composites on staphylococcus aureus. Nanotechnology. 2011; 22:135101, 9. [PubMed: 21343644]
42. Bohren, CF.; Huffman, DR. Absorption and scattering of light by small particles. Wiley; New York: 1998.
43. Šileikaitė A, Puišo J, Prosyčevas I, Tamulevičius S. Investigation of silver nanoparticles formation kinetics during reduction of silver nitrate with sodium citrate. Materials Science (Medžiagotyra). 2009; 15(1):21–27.
44. Kim J-S. Reduction of silver nitrate in ethanol by poly (*N*-vinylpyrrolidone). J Ind Eng Chem. 2007; 13(4):566–570.
45. Skrabalak SE, Chen J, Au L, Lu X, Li X, Xia Y. Gold nanocages for biomedical applications. Adv Mater. 2007; 19:3177–3184. [PubMed: 18648528]
46. International Centre for Diffraction Data. Powder diffraction files: JCPDS card numbers 41-1402 and 04-0783
47. Pragatheeswaran A, Kareem TA, Kaliani AA. Effect of plasma exposure on silver nanoparticles embedded in polyvinyl alcohol. J Phys Conf Ser. 2010; 208:012109.

48. Ferrando R, Baletto R. Structural properties of nano-clusters: energetic, thermodynamic and kinetic effects. Rev Mod Phys. 2005; 77:371–423.

49. Ajayan PM, Marks LD. Quasimelting and phases of small particles. Phys Rev Lett. 1998; 60:585–587. [PubMed: 10038590]

50. Marks LD. Experimental studies of small particle structures. Reports in Progress in Physics. 1994; 57:603–649.

51. Chang S, Chen K, Hua Q, Ma Y, Huang W. Evidence for the growth mechanisms of silver nanocubes and nanowires. J Phys Chem C. 2011; 115:7979–7986.

52. Li, LC.; Tian, Y. Zeta potential. Encyclopedia of Pharmaceutical Technology Informa Healthcare USA, Inc; 2007.

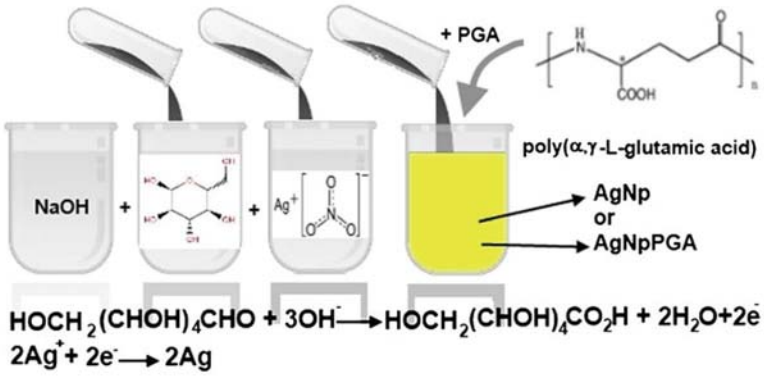

Fig. 1.
Scheme of the green synthesis of the bare and capped silver nanoparticles. *AgNp* silver nanoparticles, *AgNpPGA* silver nanoparticles capped with PGA

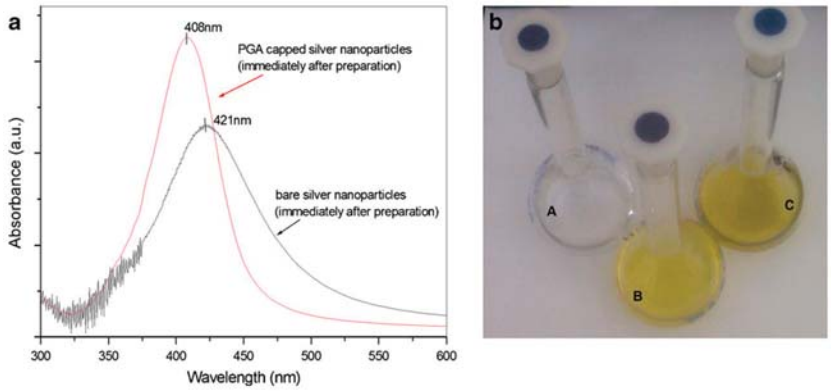

Fig. 2.

a UV–Vis spectra of bare and PGA-capped silver nanoparticles recorded immediately after preparation. **b** Digital photo showing volumetric flasks containing the negative control (*A*), bare (*B*), and capped silver nanoparticles (*C*)

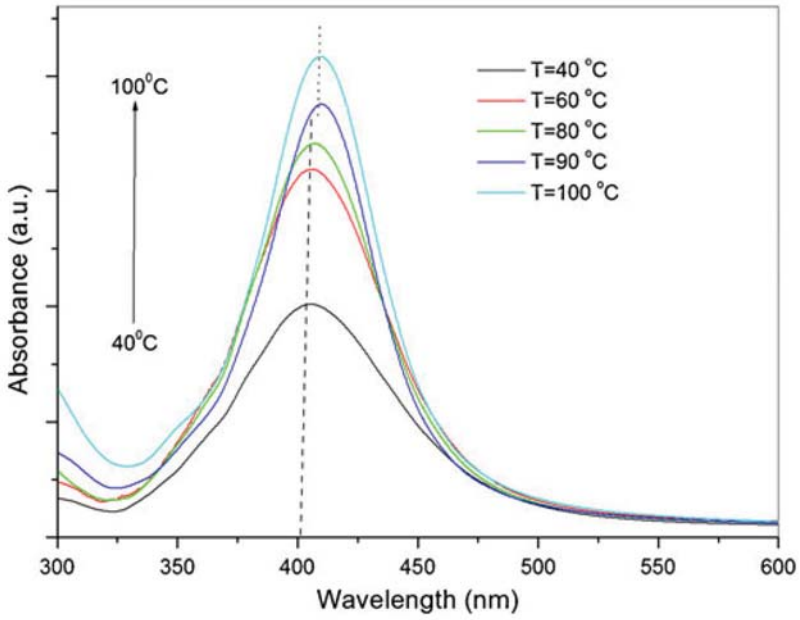

Fig. 3.
UV–Visible spectra of silver nanoparticles showing the influence of reaction temperature (reaction time, 90 min)

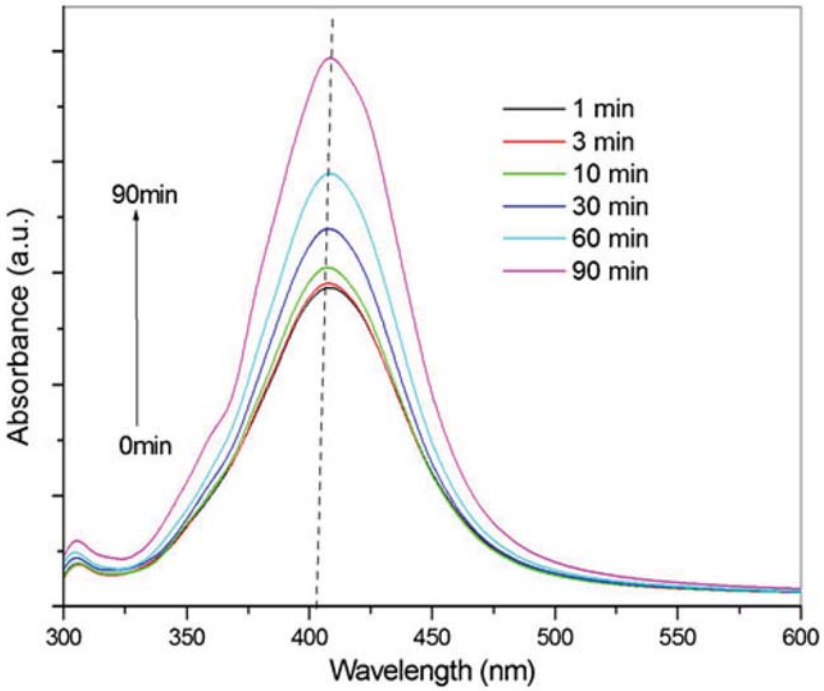

Fig. 4.
UV–Visible spectra of the PGA-capped silver particles at different times during the reaction: (*1*) 1 min, (*2*) 3 min, (*3*) 10 min, (*4*) 30 min, (*5*) 60 min, (*6*) 90 min (reaction temperature, 100 °C)

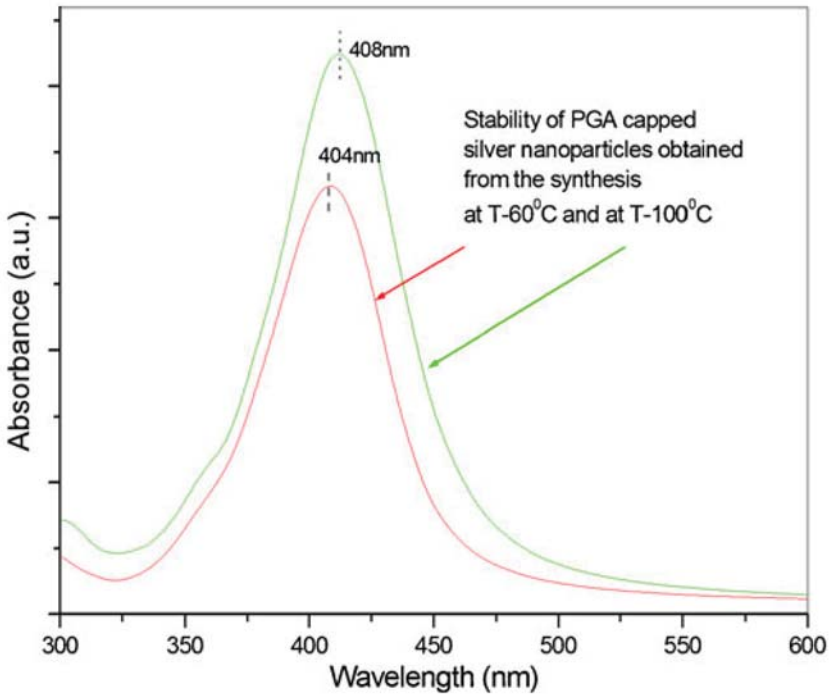

Fig. 5.
Stability of PGA-capped silver nanoparticles obtained from the synthesis at 60 and 100 °C, 3 months after the synthesis

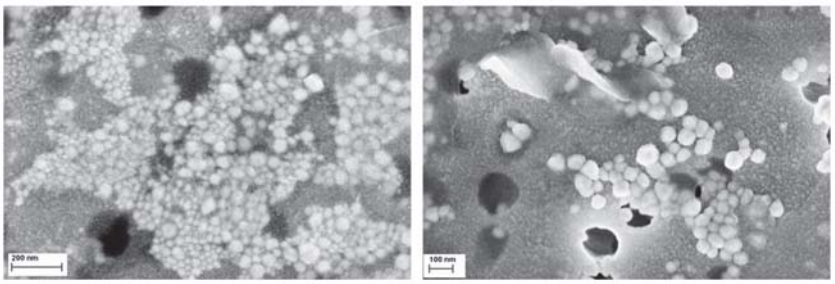

Fig. 6.
FESEM images of bare silver nanoparticles

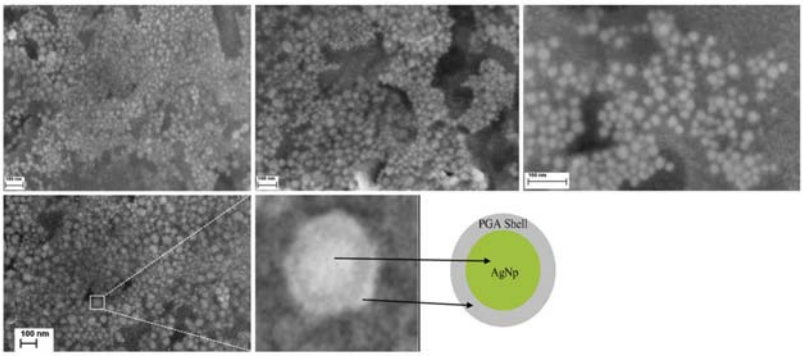

Fig. 7.
FESEM images of silver nanoparticles (*AgNp*) capped by poly(α, γL-glutamic acid) (*PGA*)

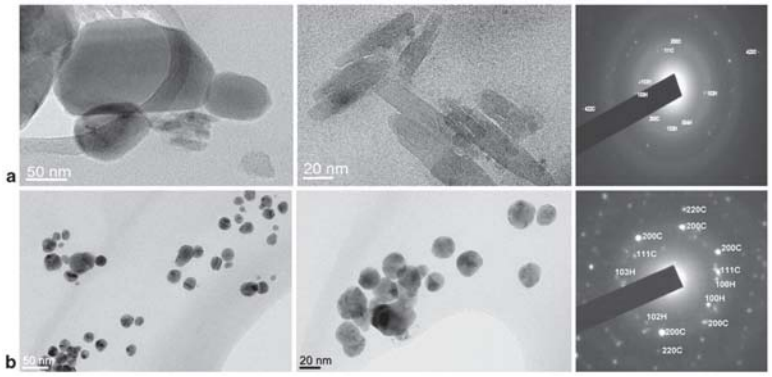

Fig. 8.
TEM images showing bare silver nanoparticles (**a**) and capped with PGA (**b**) together with the corresponding SAED patterns (*H* hexagonal, *C* cubic)

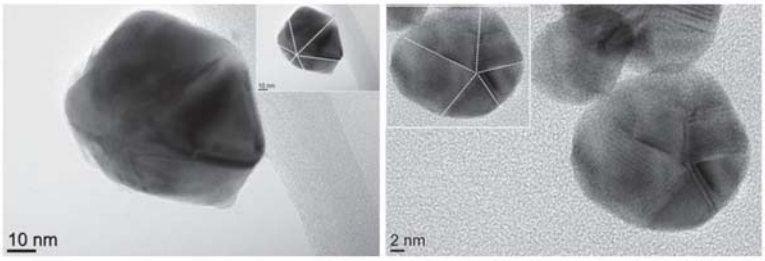

Fig. 9.
HRTEM micrographs showing multiply twinned silver nanoparticles

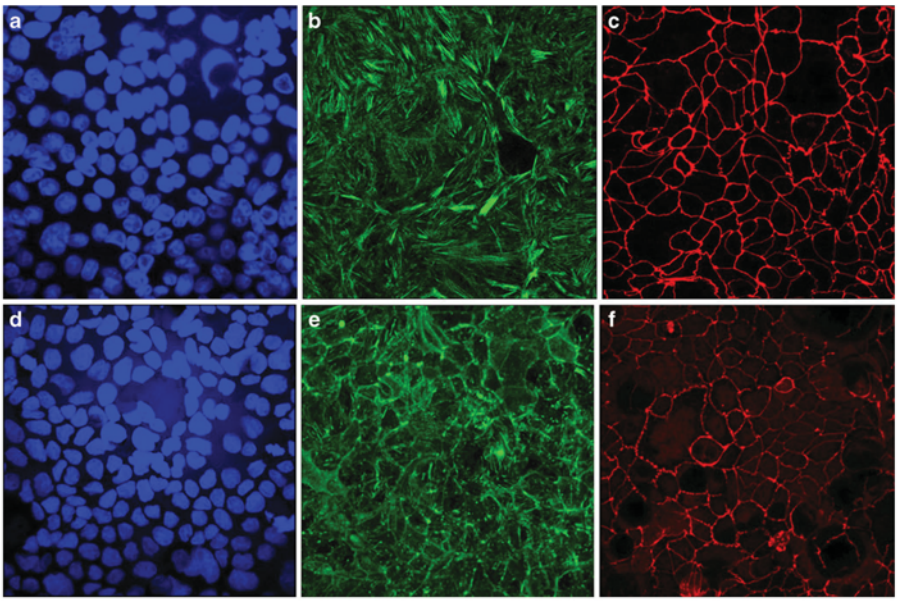

Fig. 10.

Immunoflourescence of untreated Caco-2 cells (**a**–**c**) and those following incubation with AgNpPGA (**d**–**f**) counterstained for DAPI (**a**, **d**), f-actin (**b**, **e**), and ZO-1 (**c**, **f**). All images were taken at ×60 magnification in oil. The size of each image equals 450×450 μm

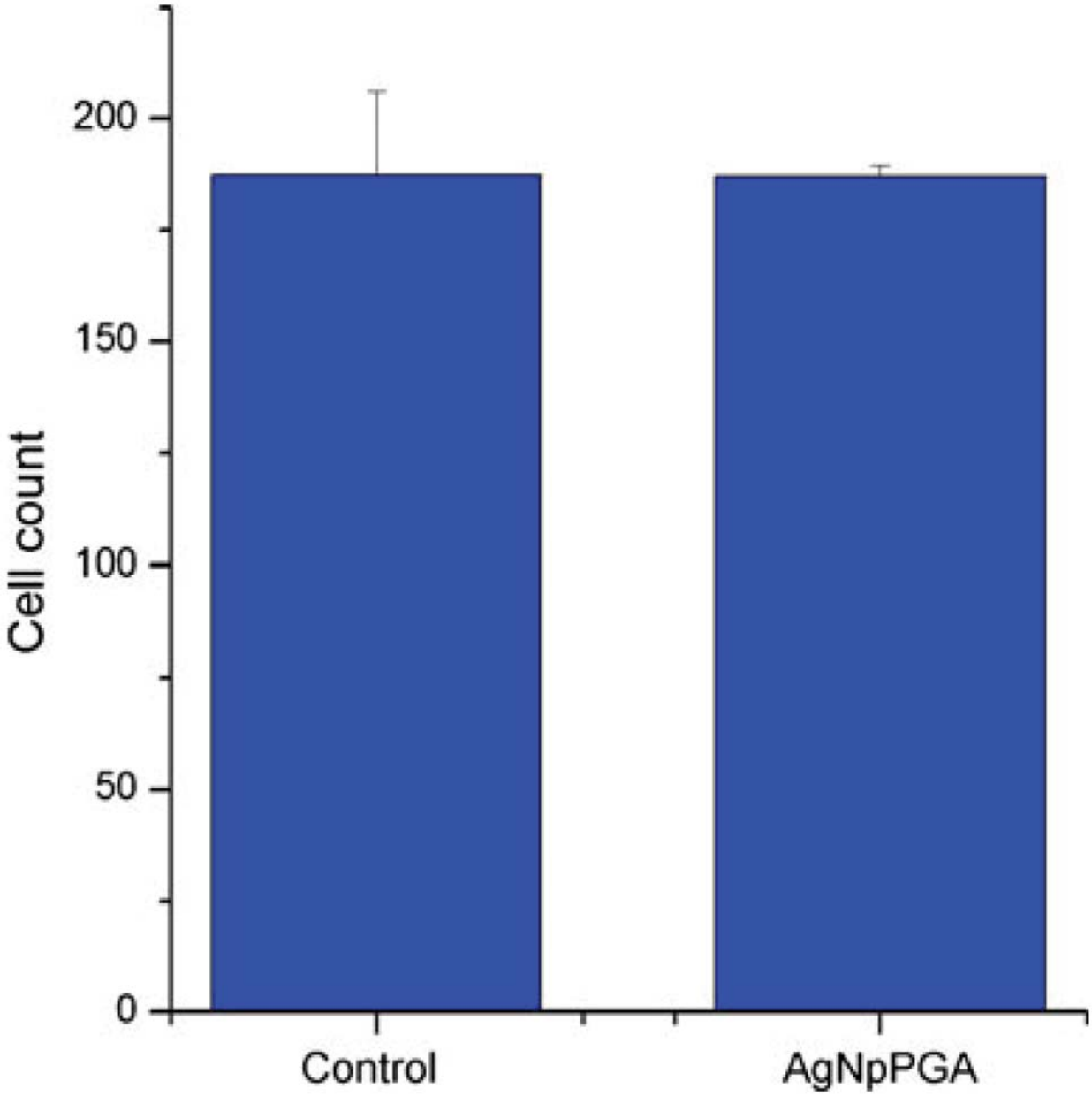

Fig. 11.
Cell count on 450×450- μm surface area (n=6) for the control Caco-2 cells and those incubated in the presence of AgNpPGA

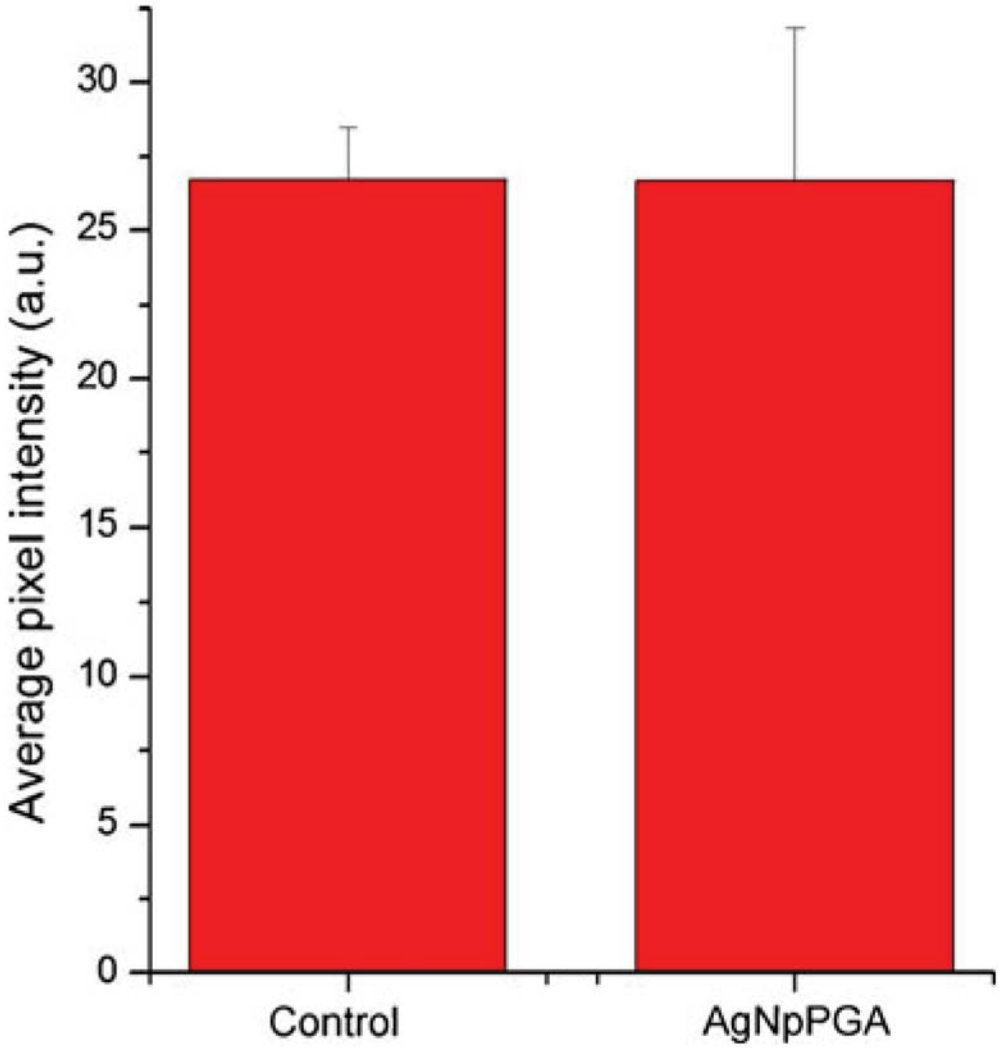

Fig. 12.
Average pixel intensity of the ZO-1-tagged fluorescent IgG (n=6) for the control Caco-2 cells and those incubated in the presence of AgNpPGA

Table 1

Zeta potential of bare and capped silver nanoparticles

Sample	Particle size (nm)	pH	Polydispersity index (PDI)	Zeta potential (mV)
Bare Ag nanoparticles	69.2±5.0	4.30–4.37	0.235	−38.5±11.5
AgNpPGA	44.9±5.0		0.206	−43.7±12.0

Values are the mean ± standard deviation (n=5)